






Article

Unveiling Urban Flood Vulnerability: A Machine Learning Approach for Mapping High Risk Zones in Tetouan City, Northern Morocco

Oussama Mekkaoui ¹, Moad Morarech ¹, Tarik Bouramtane ², Laurent Barbiero ^{3,*}, Maryem Hamidi ², Hamza Akka ⁴ and Rania Prya Muthusamy Rengasamy ⁵

¹ Laboratory of Applied and Marine Geosciences, Geotechnics and Geohazards (LR3G), Faculty of Sciences of Tetouan, University Abdelmalek Essaadi, Tetouan 93030, Morocco; oussama.mekkaoui@etu.uae.ac.ma (O.M.); mmorarech@uae.ac.ma (M.M.)

² Geoscience, Water and Environment Laboratory, Faculty of Sciences, Mohammed V University in Rabat, Avenue Ibn Batouta, Rabat 10100, Morocco; tarik_bouramtane@um5.ac.ma (T.B.); maryem_hamidi@um5.ac.ma (M.H.)

³ Institut de Recherche pour le Développement, Géoscience Environnement Toulouse, CNRS, University of Toulouse, Observatoire Midi-Pyrénées, UMR 5563, 14 Avenue Edouard Belin, 31400 Toulouse, France

⁴ Laboratory, Research & Development in Applied Geosciences, Faculty of Science and Techniques Tangier, University of Abdelmalek Essaadi, Tangier 90000, Morocco; hamza.akka@etu.uae.ac.ma

⁵ Laboratory of Intelligent Automation & Bio Med Genomics, Faculty of Science and Techniques Tangier, University of Abdelmalek Essaadi, Tangier 90000, Morocco; raniaprya.muthusamyrengasamy@etu.uae.ac.ma

* Correspondence: laurent.barbiero@get.omp.eu

Abstract: This study examines urban flood vulnerability in Tetouan city, Northern Morocco, using four machine learning models—Classification and Regression Tree (CART), Support Vector Machine (SVM), Logistic Regression (LR), and Factorial Discriminant Analysis (FDA)—to identify and map flood-prone areas. The primary goal is to enhance flood prevention efforts and minimize losses by determining the most vulnerable zones. The analysis highlights consistent flood risk along the Martil River and eastern plains, areas characterized by low-lying topography, dense drainage, proximity to canals, and recent urban development. Despite some spatial variation among the models, all consistently indicate low and very high vulnerability zones, with FDA identifying the highest proportion of very high risk areas (58%), followed by CART, SVM, and LR (39%, 38%, and 37%, respectively). In terms of model accuracy, SVM and LR outperform others, demonstrating their effectiveness in flood risk delineation. The findings offer valuable insights for urban planners and decision-makers in flood risk management, contributing to more informed resource allocation in Tetouan-Martil and potentially guiding similar strategies in comparable regions globally.

Keywords: flood vulnerability; machine learning models; urban planning; risk management; Tetouan



Academic Editor: Dario Domingo

Received: 16 December 2024

Revised: 5 February 2025

Accepted: 25 February 2025

Published: 4 March 2025

Citation: Mekkaoui, O.; Morarech, M.; Bouramtane, T.; Barbiero, L.; Hamidi, M.; Akka, H.; Rengasamy, R.P.M. Unveiling Urban Flood

Vulnerability: A Machine Learning Approach for Mapping High Risk Zones in Tetouan City, Northern Morocco. *Urban Sci.* **2025**, *9*, 70.

<https://doi.org/10.3390/urbansci9030070>

Copyright: © 2025 by the authors. Licensee MDPI, Basel, Switzerland. This article is an open access article distributed under the terms and conditions of the Creative Commons Attribution (CC BY) license (<https://creativecommons.org/licenses/by/4.0/>).

1. Introduction

From 2000 to 2019, floods accounted for 44% of all disasters, affecting 1.6 billion people worldwide [1–6]. The combined effects of climate change and rapid urbanization exacerbate the frequency and severity of these floods, putting communities at risk and causing disruptions in transportation, damage to infrastructure, and destruction of property [7–10].

Urban floods are classified as a major global natural disaster, causing approximately 20,000 deaths each year [6]. They are a distinct form of flooding triggered by inadequate

drainage systems within urban environments. During heavy rainfall events or prolonged rainy periods, runoff can exceed the capacity of drainage infrastructure, leading to such floods [11]. In developing countries, rapid and unregulated urbanization often results in human encroachment into active channels, altering the morphology of drainage networks and thus promoting urban flooding [12].

Cities in northern Morocco are particularly affected due to annual precipitation amounts (600 to 1000 mm) influenced by oceanic conditions, combined with a Mediterranean climate characterized by violent storms [13,14]. Ongoing climate change poses an additional threat to coastal urban environments, with observed sea level rise (between 3.2 and 4.2 mm/year over the period 2006–2018) and an increase in the frequency of extreme rainfall events [15,16].

To minimize the damage caused by these floods, it is essential to develop vulnerability maps of urban areas, a topic widely studied in recent scientific and technical literature [17]. The success of risk assessment heavily depends on the modelling methods used. While traditional physical models such as HEC-RAS and AutoRoute have proven effective [9,18–21], machine learning techniques such as support vector machines, decision trees, logistic regression, and linear discriminant analysis are gaining popularity for predicting natural hazards in data-limited environments.

The emergence of advanced geographic data collection and analysis techniques offers promising solutions to the challenges of urban flooding, particularly by integrating complex factors such as climate change and urban characteristics. Machine learning algorithms can significantly contribute to optimizing real-time flood management strategies [17,22–24].

The aim of this study is to use a combination of machine learning techniques to evaluate the vulnerability of urban flooding in the coastal and tourist city of Tetouan, which is experiencing rapid development. Vulnerability mapping is carried out by applying four distinct machine-learning models, and their effectiveness, accuracy, and performance are evaluated and compared using statistical validation indices.

2. Materials and Methods

2.1. Study Area

Tetouan is a coastal city of approximately 200,000 inhabitants located in the lower valley of the Martil River in northern Morocco (Figure 1) [25]. It is nestled between several mountains, namely the Rif of Jbel Dersa to the north, Jbel Ghorghiz to the south, and the Ouadrasse hills to the west [26]. The Rif mountains form a natural barrier between the Mediterranean coast and the interior of the country, influencing the hydrological characteristics of the region and water resources. They are mainly composed of Jurassic and Cretaceous limestones, sandstones, and shales [26]. The Mediterranean climate is characterized by two distinct seasons: a cool and wet season from October to April, where 92% of the total precipitation (600 to 800 mm) occurs, and a hot and dry season from May to September [27]. The steep slopes lead to rapid runoff during heavy rains, causing periodic flooding in some parts of the city, mainly during the winter months (Figure 2) [28]. Low incomes, high unemployment rates, and inadequate housing increase vulnerability to urban flooding.

Tetouan is, however, a central economic hub in the region with diverse activities in agriculture, industry, and services. It is also a prominent tourist destination, offering a wealth of historical sites and cultural attractions, some of which were recognised by e.g., UNESCO-WHC, 2021.

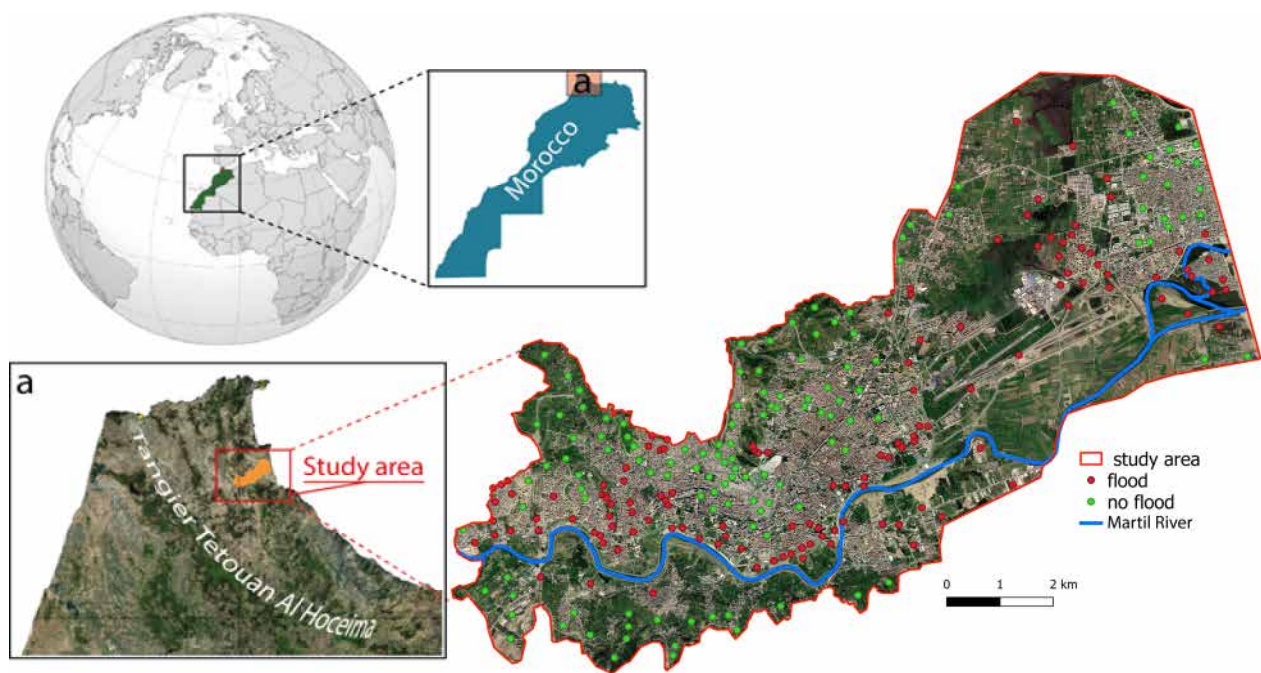


Figure 1. Satellite view of study area and the locations of flooded and unflooded points, within (a) Tangier Tetouan Al-Hoceima region.



Figure 2. (a–e) Examples of flooded streets and infrastructures in Tetouan city during 2020 and 2024 floods.

2.2. Data Collection and Description

The study was based on an inventory of locations recently affected by the floods, using social networks and the local press (social media) that accompanied the events, and then

supplemented by a field survey to gather precise information from eyewitnesses present or living in the affected neighbourhoods. This inventory resulted in the identification of 120 points exposed and 120 not exposed to flooding; giving a total of 240 points. The inventory was positioned on a Digital Elevation Model (DEM) with a resolution of 30 m (ASTER DEM). Finally, nine geo-environmental factors were identified, followed by four socio-environmental factors based on demographic databases, all of which are likely to contribute to or control flooding in the study area [25]. All the data is managed using QGIS3.20 software.

2.3. Selected Parameters

A wide range of interconnected factors influences urban flooding, yet no standardized guidelines exist for their selection due to the complexity of the phenomenon. This study leverages remote sensing and GIS techniques, combined with insights from previous research and available local data, to identify key geo-environmental and socio-environmental factors relevant to urban flooding. These factors were chosen based on their significance in influencing flood dynamics and their accessibility within the study area. The integration of these datasets provides a robust framework for analyzing flood risks, offering valuable insights for urban planning and flood mitigation strategies.

2.3.1. Geo-Environmental Factors

Floods are influenced by a complex interplay of geo-environmental factors that shape the dynamics of water flow, accumulation, and inundation. Understanding these factors is critical for assessing flood susceptibility and implementing effective risk management strategies. This study examines key geo-environmental parameters derived from Digital Elevation Model (DEMs) and other geospatial tools to identify their roles in flood processes.

Elevation (Figure 3a) of the study area, the majority lies at low altitudes, ranging from 0 to 337 m. These low-lying regions, often near floodplains or coastal zones, are particularly vulnerable to flooding due to slower water drainage and increased accumulation. Elevation influences the direction and speed of water flow, as well as the extent of inundation, making it a key parameter for assessing flood susceptibility.

Slope (Figure 3b) is a major physiographic feature for flooding contributing directly to runoff velocity and sediment transport. It was generated from the DEM layer using QGIS tools that calculates for each cell the maximum rate of change in elevation values relative to its neighbors. Slopes ranged from 0° to 90°.

The exposition parameter (Figure 3c) is defined as the direction of the maximum slope of the earth's surface. It influences microclimate, sun exposure time, moisture retention, evapotranspiration, rock weathering, vegetation cover and denudation processes, i.e., it indirectly affects flooding. This parameter was also generated from the DEM layer using QGIS tools.

The curvature (Figure 3d, unitless) of the land surface is a useful runoff factor for detecting flood susceptibility. It was divided into three categories, namely concave (positive values, where water tends to accumulate), convex (negative values, where water typically tends to flows) and flat surface.

The Topographic Position Index TPI (Figure 3e, unitless) indicates the upper and lower parts of the landscape, i.e., the difference in altitude of each cell in relation to the average altitude of the surrounding cells. Positive values indicate areas above the surrounding cells, i.e., ridges, while values near zero generally represent flat terrains, and finally negative values indicate areas below the surrounding cells, i.e., valleys.

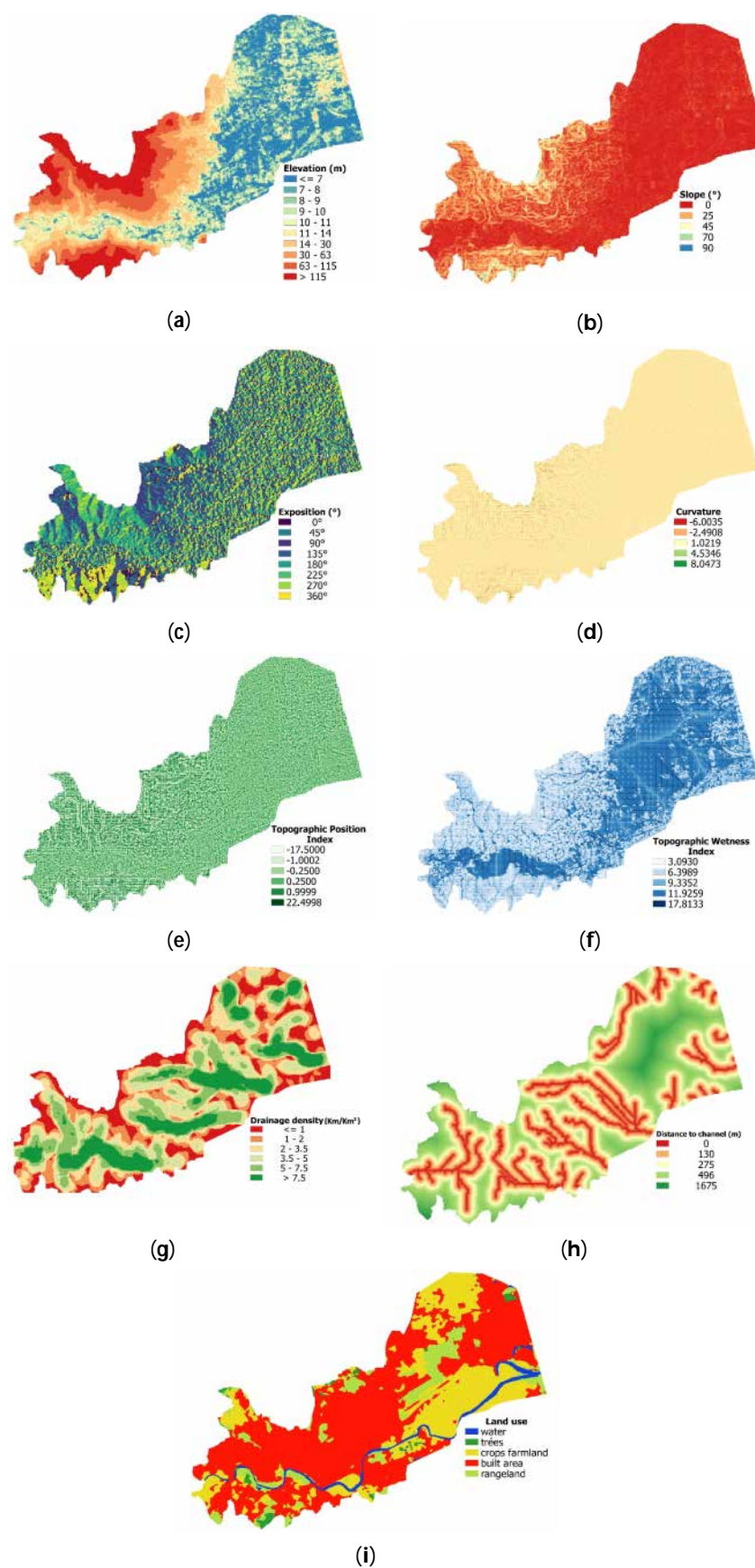


Figure 3. Maps of geo-environmental factors of the study area (a) Elevation, (b) Slope, (c) Exposition, (d) Curvature, (e) Topographic Position Index (TPI), (f) Topographic Wetness Index (TWI), (g) Drainage density, (h) Distance to channel, (i) Land use.

The Topographic Wetness Index TWI (Figure 3f, unitless) reflects the amount of water accumulated in each pixel of the watershed. In other words, it reflects the effect of topography on the spatial distribution of sources saturated to generate runoff. The TWI is also expressed as the power of surface runoff, such as flow velocity, transport capacity and potential flow. Typically, it ranges from 2 to 6 in steep, well drained areas, and can exceed 10 in flat or low-laying regions with significant water accumulation potential. It was generated using Grass 7.6.1 GIS tools.

Drainage density (km/km^2 , Figure 3g) represents the length of watercourses in kilometres per unit area in square kilometres (km^2). It reflects the permeability of the soil surface and the infiltration rate, and therefore controls the intensity of runoff, which is directly linked to flooding. It was calculated from the drainage network using the linear density tool in the QGIS software.

The distance to channel (Figure 3h) determines the preponderant role of a dense hydrological network in the occurrence of floods. It represents the distance between the point of flooding and the drain. It was calculated using the Euclidean distance tool in GIS software.

Land use (Figure 3i) has a strong influence on many types of natural hazards, including flooding. This land-use map of Tetouan-Martil obtained from the Sentinel-2 imagery satellite of the European Space Agency (ESA) at 10 m resolution. This annual Land-Use map generated using artificial intelligence, using a supervised massive training dataset.

2.3.2. Socio-Environmental Factors

The socio-environmental factors associated with the study area are primarily derived from demographic datasets for the Tangier-Tetouan-Al Hoceima region, as published by the Moroccan Haut Commissariat au Plan [25]. These factors provide critical insights into human-environment interactions and their contribution to flood risk, emphasizing the need for urban planning and management strategies.

Building density: This parameter evaluates the concentration of structures within a given area, subdivided into four classes—very low, low, medium, and high. Very low density areas are predominantly rural or sparsely built, with large open spaces. Low density areas are characterized by scattered development, such as suburban zones. Medium density areas feature a balanced mix of residential and commercial buildings, while high density areas represent densely populated urban centres with compact construction patterns (Figure 4a).

Population density: This parameter is divided into four classes—low, medium, high, and very high (Figure 4b). Low density zones are characterized by scattered populations, such as rural communities. Medium density areas include moderately populated suburban neighbourhoods. High density zones are typically urban areas with substantial residential and commercial activity, while very high density zones represent central urban cores or heavily populated districts.

Building types: Structures are classified into eight categories to reflect diverse land-use patterns in the region (Figure 4c): Residential areas, zones primarily composed of housing units for urban or suburban populations. Apartment zones, densely packed housing complexes. Industrial areas, regions allocated for manufacturing, warehouses. Construction areas, active sites of new building projects or infrastructure development. Farmland areas, agricultural zones dedicated to crop cultivation. Forest areas, regions covered by natural or planted vegetation. Bare land, undeveloped areas with no vegetation or human activity. Cemeteries, areas designated for burial purposes, typically with minimal structural development.

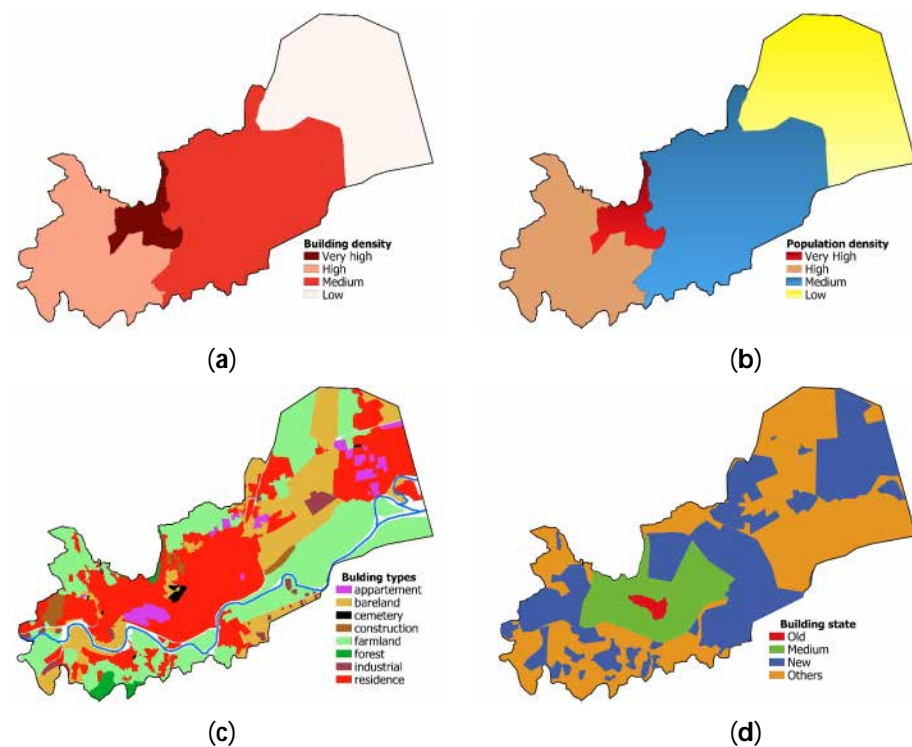


Figure 4. Maps of socio-environmental factors of the study area (a) Building density; (b) Population density; (c) Building types; (d) Building state.

Building state: In Tetouan, buildings are categorized into four distinct conditions based on their age and state of repair (Figure 4d): Recently constructed buildings, structures completed between six and fifteen years ago, typically in good condition and meeting modern construction standards. Older buildings, structures that were completed more than fifteen years ago and may exhibit moderate signs of wear and aging. Old and deteriorated buildings, refers to structures located in the historic medina or those in an advanced state of disrepair, often posing significant risks during extreme weather events due to structural vulnerabilities. Vacant land, areas with no built structures, representing potential sites for urban expansion or green space development.

2.4. Data Analysis and Modelling

Four machine learning approaches were used to establish flood vulnerability, namely (1) Factor Discriminant Analysis (FDA), (2) Logistic Regression (LR), (3) Classification and Regression Tree (CART), and (4) Support Vector Machine (SVM).

Discriminant Factor Analysis is an interpretative and predictive statistical method involving a defined qualitative variable [29,30]. In addition to factor analysis, it is a supervised classification method. The aim is to describe, explain and predict the membership of a group or class of a set of observations (flood, landslide, etc.) based on a series of predictor variables (latitude, slope, exposure, drainage density, type of building, etc.).

Logistic regression is a statistical method for analysing a set of data in which one or more independent variables determine a result. The aim is to find the model best suited to describing the relationship between the dependent and independent variables. Here a logistic regression model was used to predict the probability of occurrence (score = 1) or non-occurrence (score = 0) of an urban flood, based on the optimisation of the regression coefficients. This score always varies between 0 and 1. If the predicted value is above a given threshold, the event is likely to occur, whereas if the predicted value is below the same threshold, the event will not occur [12].

Classification and regression trees, first introduced by [31,32], are efficient and powerful methods for addressing classification problems [33], and have been successfully applied to urban flood classification [12]. Their application involves four key steps: (1) building the tree, where the data is split recursively based on decision rules to maximize classification accuracy; (2) stopping tree building, which occurs when further splits fail to provide significant improvement in classification, typically determined by thresholds for impurity reduction or information gain to avoid overfitting; (3) pruning the tree, where unnecessary branches are removed to simplify the model and enhance generalizability; and (4) selecting the optimal tree, which balances complexity and performance to effectively classify flood or no-flood classes [34].

The support vector machine is a supervised machine learning technique that was developed in the context of statistical learning theory [35]. It has been shown to be more effective than several other machine learning methods in modelling natural hazards and identifying areas at risk [12,24,33,36]. Its objective is to find an optimal hyperplane (or decision boundary) in an N-dimensional space (where N is the number of variables) that distinctly classifies floodable and non-floodable points. The optimal linear hyperplane is used to separate the original input space, and the kernel function is used to transform the data into two classes made up of at-risk and non-at-risk points (0, 1). SVM performance depends on appropriate kernel functions, including Polynomial kernel (PL), Sigmoid Kernel (SK), Radial Basis Function (RBF) and Linear Kernel (LN). According to several studies [37,38], the RBF outperforms the other kernels in flood forecasting. It is this RBF function that has been used here [24,36].

The selection of these methods is based on their proven efficiency and widespread use in mapping susceptibility and vulnerability to natural hazards. Their simplicity in construction, use, and interpretation, combined with straightforward optimization, makes them particularly suitable for this type of analysis.

For each method, hyper-parameters were automatically optimized through integrated algorithms to ensure optimal settings during training, which was performed on 70% of the dataset. For instance, Factor Discriminant Analysis (FDA) adjusts the coefficients of discriminant variables to simplify the process. Logistic regression optimizes parameters such as the type of regularization (L1 or L2) and the convergence threshold. Classification and Regression Tree (CART) adjusts criteria like tree depth, the minimum number of samples per leaf, and the splitting criterion, such as Gini index or entropy. Finally, Support Vector Machine (SVM) optimizes parameters like regularization (C), kernel type (linear or RBF), and, for non-linear kernels, the gamma parameter. Figure 5 shows a flowchart simplifying the methodological approach to modelling and mapping areas vulnerable to urban flooding.

2.5. Model Validation Methods

2.5.1. Repeated Hold-Out Method

The Hold-Out method is a commonly used technique for validating machine learning models [39]. It divides a data set into two parts, one for training and the other for validation. The repeated Hold-Out method is a variant. It overcomes its limitations by averaging model performance over several iterations with different data partitions [40]. This provides a more stable estimate of model performance [41,42]. Here, we used the Repeated Hold-Out method, with 10 random partitions of data, 70% for training and 30% for validation. The four machine learning methods are trained on the training set and validated on the test set for each partition, with the performance of each model calculated using the arithmetic mean Equation (1):

$$\bar{P} = \frac{1}{k} \sum_{i=1}^k P_i \quad (1)$$

where P represents the average value of a performance metric, which can be the total accuracy of the model or other metric; k is the number of splits (where $k = 10$); and P_i is the result of the performance metric of each split.

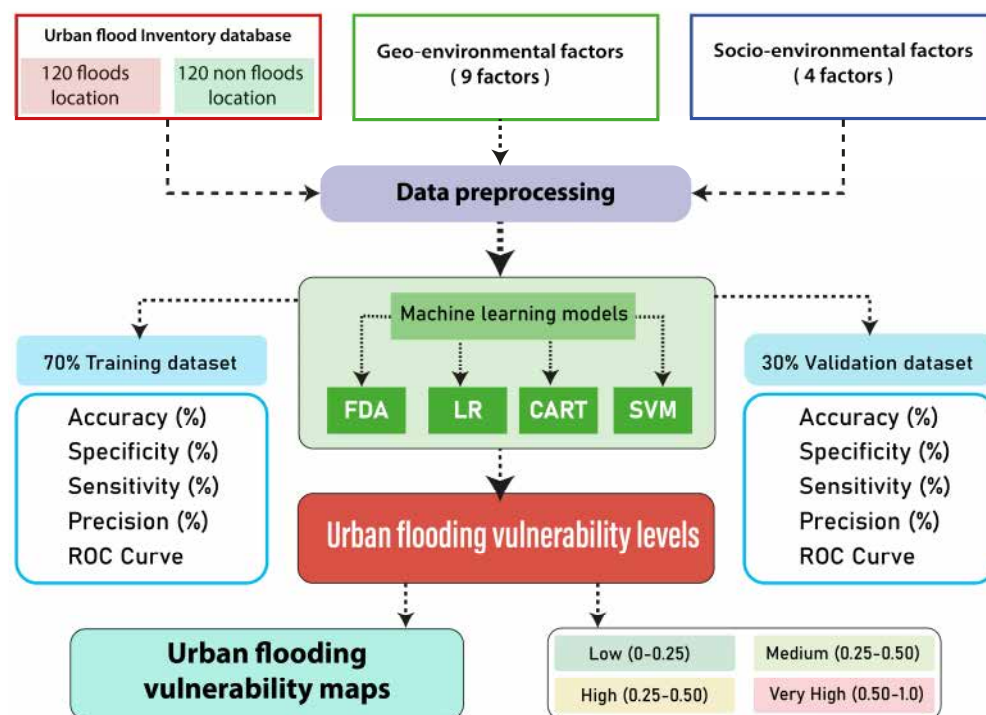


Figure 5. Flow chart of the adopted methodology for preparing flood vulnerability maps.

2.5.2. Performance Metrics and Evaluation Criteria

The performance of the classification models was evaluated using the confusion matrix (Table 1) by comparing the model's predicted results with the actual results, based on four criteria: ACCuracy (ACC; Equation (2)), SenSiTivity (SST; Equation (3)), SPeciFicity (SPF; Equation (4)), and PReCision (PRC; Equation (5)) [43]. Higher values of ACC, SST, SPF, and PRC indicate better model performance [44]. The models were also evaluated using Receiver Operating Characteristic (ROC) curve statistics, which measure the model's ability to distinguish between flood-prone and non-flood-prone areas. Unlike accuracy, which assesses overall correctness, the ROC curve evaluates the trade-off between true positive and false positive rates across different classification thresholds. It is widely used as a standard metric for assessing spatial modeling performance. The ROC-AUC value represents the probability that a randomly chosen positive instance (flood occurrence) is ranked higher than a randomly chosen negative instance (no flood occurrence). Based on ROC curve statistics, models were classified as poor (0.5–0.6), fair (0.6–0.7), good (0.7–0.8), very good (0.8–0.9), and excellent (0.9–1).

$$ACC = \frac{TP + TN}{TP + TN + FN + FP} \quad (2)$$

$$SST = \frac{TP}{TP + FN} \quad (3)$$

$$SPF = \frac{TN}{TN + FP} \quad (4)$$

$$\text{PRC} = \frac{\text{TP}}{\text{TP} + \text{FP}} \quad (5)$$

Table 1. Confusion matrix of a binary classification.

	Predicted Positive	Predicted Negative
Observed Positive	True Positive (TP)	False Negative (FN)
Observed Negative	False Positive (FP)	True Negative (TN)

2.6. Contribution Analysis of Parameters

The relative contribution of the variables was assessed using the Jackknife test [45], which involves sequentially removing one predictive variable at a time and recalculating the performance of each model to examine the amount of bias or information lost due to the removal of that variable. The sensitivity of each indicator is assessed by the percentage Decrease in overall ACCuracy (DACC).

$$\text{DACC}_i = \frac{\text{ACC}_{\text{All}} - \text{ACC}_i}{\text{ACC}_{\text{All}}} \times 100 \quad (6)$$

where ACC_{All} represents the calculated value of the overall accuracy of the model using all parameters. ACC_i denotes the ACC value of the model when parameter i is removed from the input dataset, and DACC_i is the corresponding percentage decrease in ACC.

3. Results

3.1. Urban Flood Vulnerability Mapping

Using Geographic Information System (GIS 3.20) software, we developed four urban flood vulnerability maps utilizing the CART (Classification and Regression Trees), SVM (Support Vector Machine), LR (Logistic Regression), and FDA (Factorial Discriminant Analysis) algorithms. Figure 6 presents a flood vulnerability assessment for the Tetouan-Martil study area, classifying flood risk into four categories: low (0–0.25), medium (0.25–0.5), high (0.5–0.75), and very high (0.75–1). This threshold is the most applicable and represents the probability of an area being vulnerable to flooding, with 0 being no vulnerability and 1 being maximum vulnerability. The results from all four modelling algorithms exhibit similar patterns of flood vulnerability (Figure 6). Notably, the areas classified as having a very high flood probability contain the majority of the flood points identified during post-flash flood field surveys. In contrast, areas with the lowest vulnerability of flooding include most of the non-flood points, further validating the accuracy of the models. Although each algorithm captures different spatial nuances, all the models consistently identify flood-prone zones concentrated along the Martil River, which flows through the study area from west to east. The eastern plain of the study area is particularly susceptible to flooding. These high risk areas are primarily associated with low elevation, high drainage density, proximity to water channels, and recent construction developments (Figure 6).

Regarding the spatial distribution of areas with high and low flood exposure, all the vulnerability maps produced similar results, with the exception of the FDA model, which identified a significantly larger portion of the study area as highly flood-prone. Among the models, the FDA proved to be the most discerning, estimating that 58% of the study area is at very high risk of flooding. In comparison, the SVM model estimated 39%, while the CART and LR models provided slightly lower estimates of 38% and 37%, respectively (Figure 7).

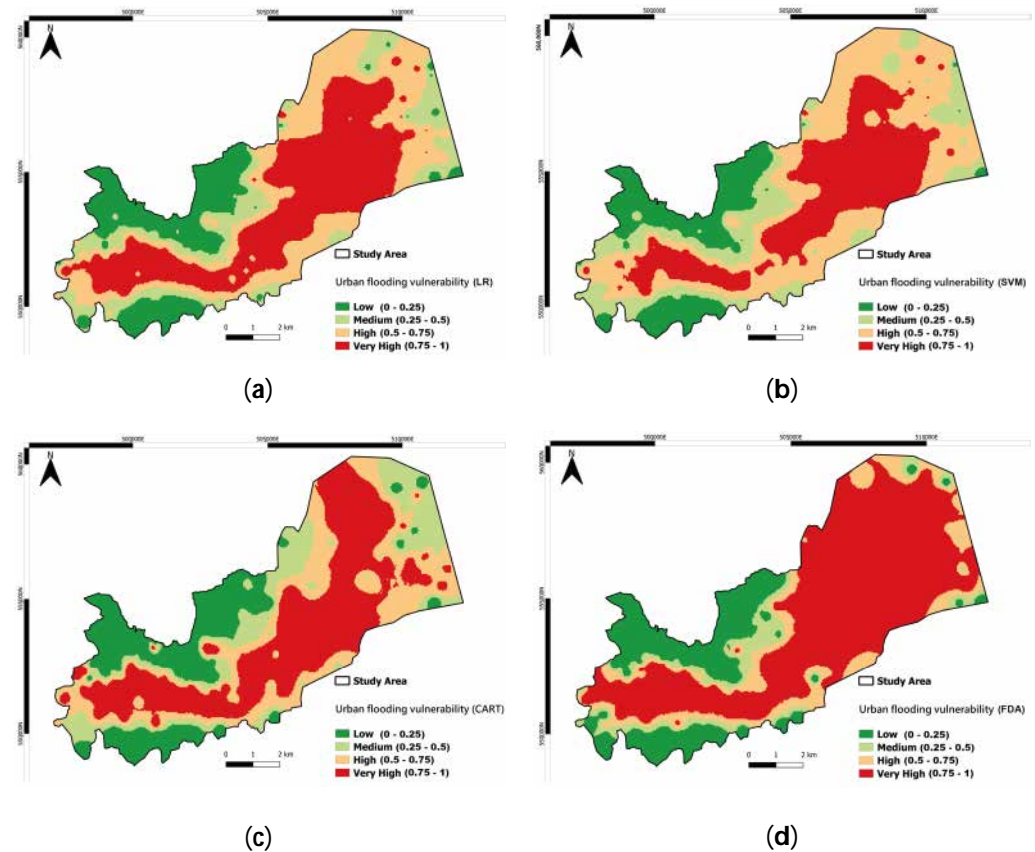


Figure 6. Urban flooding vulnerability maps obtained from (a) Logistic Regression (LR); (b) Support Vector Machine (SVM); (c) Classification and Regression Tree (CART) and (d) Factorial Discriminant Analysis (FDA).

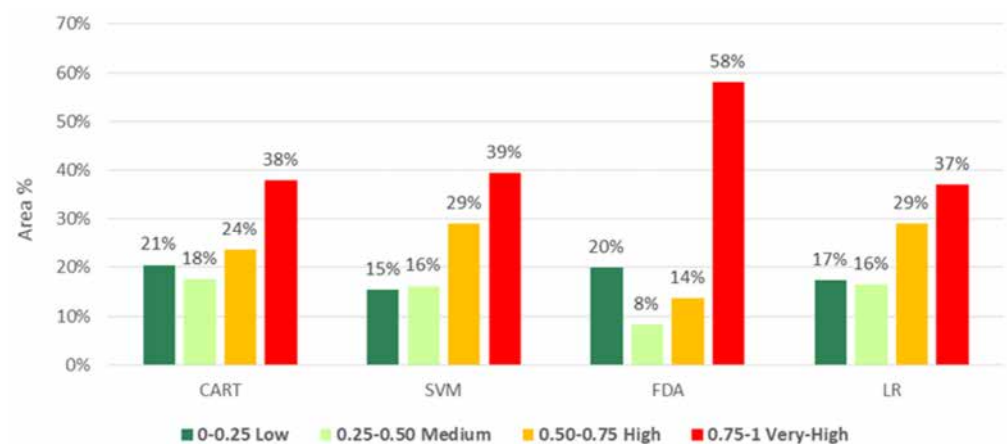


Figure 7. Percentage of area occupied by each vulnerability class determined by the four models over the study area: Classification and Regression Tree (CART); Support Vector Machine (SVM); Factorial Discriminant Analysis (FDA); Logistic Regression (LR).

3.2. Contribution of Factors to Susceptibility Mapping

The evaluation of explanatory variables provides valuable insights into urban flooding issues and offers environmental managers a practical framework for resource allocation and planning in natural resource management. Although the vulnerability zones and their distributions were largely similar, the contributing factors varied across models. The CART model (Figure 8a) relied almost exclusively on elevation as the primary determinant, i.e., in this case, elevation played a key role in defining flood-prone areas. In the SVM model (Figure 8b), drainage density emerged as the most significant factor, followed

by elevation, exposure, and slope. The FDA model (Figure 8c) prioritized elevation, slope, and drainage density as the top three contributing parameters. Using Factorial Discriminant Analysis (FDA), these three variables were crucial in shaping the flood susceptibility analysis. Elevation, slope, exposure, and curvature together shaped the LR model predictions (Figure 8d). Across all four models, socio-environmental factors—such as building density, population density, building type, and building condition—had little influence on the flood risk predictions.

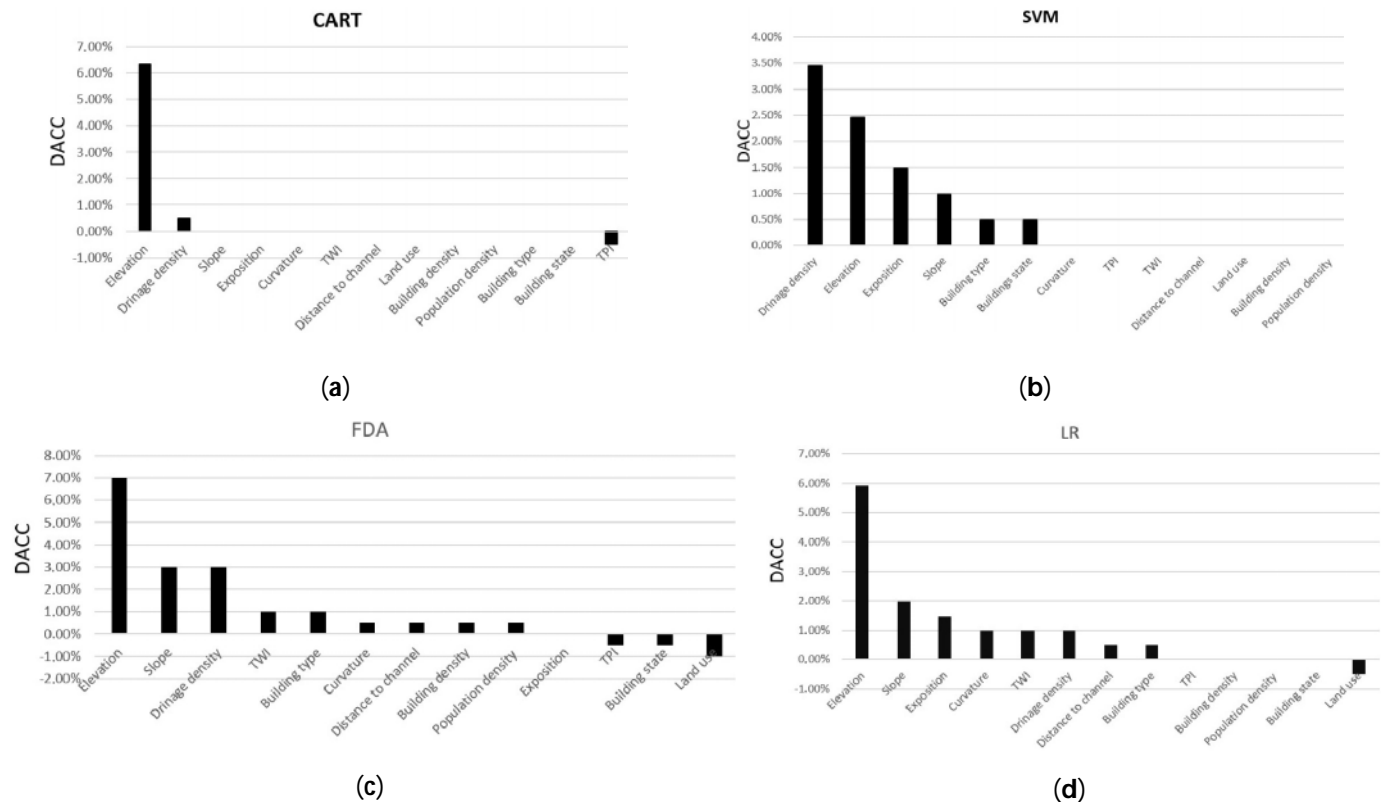


Figure 8. Contribution of descriptive parameters for each model (DACC %, Equation (6)) for (a) Classification and Regression Tree (CART), and (b) Support Vector Machine (SVM), (c) Factorial Discriminant Analysis (FDA), (d) Logistic Regression (LR).

3.3. Model Validation for Flood Vulnerability Prediction

The comparison of the four urban flood models—LR, CART, SVM and FDA—provides valuable insights into their performance, based on statistical analyses of both training (Table 2) and testing (Table 3) datasets. LR consistently performed well, achieving an accuracy of 84.88% during training and 80.83% during testing. It showed balanced metrics across the board: specificity (84.57% in training, 78.81% in testing), sensitivity (85.15% and 82.94%), precision (84.81% and 79.33%), and ROC-AUC (0.93 and 0.90). This level of consistency reflects strong generalization, meaning the model is capable of handling new, unseen data with minimal performance degradation.

CART, on the other hand, achieved high accuracy during training (85.95%) but suffered a notable drop in testing accuracy (79.17%), indicating overfitting. Overfitting occurs when a model is too closely tailored to the training data, resulting in a weaker performance on unseen data. This was evident in CART's drop in specificity (85.8% to 77.3%), sensitivity (86.1% to 81.3%), precision (86.6% to 77.6%), and ROC-AUC (0.92 to 0.83).

SVM demonstrated only moderate declines from training to testing: accuracy (84.82% to 80.69%), specificity (85.8% to 81.5%), sensitivity (83.9% to 79.8%), precision (85.8% to

80.6%), and ROC-AUC (0.92 to 0.89). This reflects good generalization, as the model maintains its effectiveness on new data with minimal reductions in performance.

Table 2. Predictive capability of urban flood models using the training dataset.

Statistical Index	FDA	LR	CART	SVM
Accuracy (%)	83.87%	84.88%	85.95%	84.82%
Specificity (%)	75.75%	84.57%	85.76%	85.77%
Sensitivity (%)	91.79%	85.15%	86.08%	83.86%
Precision (%)	79.52%	84.81%	86.61%	85.81%
ROC Curve	0.94	0.93	0.92	0.92

Table 3. Predictive capability of urban flood models using the testing dataset.

Statistical Index	FDA	LR	CART	SVM
Accuracy (%)	74.03%	80.83%	79.17%	80.69%
Specificity (%)	69.94%	78.81%	77.33%	81.47%
Sensitivity (%)	77.56%	82.94%	81.26%	79.76%
Precision (%)	72.51%	79.33%	77.56%	80.59%
ROC Curve	0.94	0.90	0.83	0.89

FDA, despite having the highest ROC-AUC values (0.94 in training and in testing), showed significant declines in other performance metrics such as accuracy (83.9% to 74%), specificity (75.8% to 69.9%), sensitivity (91.8% to 77.6%), and precision (79.5% to 72.5%). These drops suggest that FDA may suffer from overfitting, excelling on training data but failing to generalize to new data. While the high ROC-AUC reflects its ability to distinguish between classes, it does not guarantee overall prediction accuracy. The sharp declines in other metrics indicate the model may be overly complex or sensitive to noise, requiring refinement to improve generalization.

In conclusion, LR and SVM emerged as the most reliable models due to their balanced trade-off between accuracy and ROC-AUC, ensuring both strong predictive power and generalization capability. Unlike FDA and CART, which achieved the highest ROC-AUC but exhibited a significant drop in accuracy, LR and SVM maintained stable performance across all metrics, with accuracy above 80% and ROC-AUC around 0.90. This consistency indicates that they effectively classify flood-prone areas while minimizing misclassifications. Meanwhile, CART and FDA required further refinement and validation, as their performance showed signs of overfitting and instability, leading to reduced reliability when applied to new data.

The performance of these models was further validated during the flooding event that struck the Tetouan region from 30 March to 1 April 2024. This catastrophic event, marked by intense rainfall (recording a pluviometry of 121 mm in Tangier Tetouan Alho-ceima), caused widespread flooding, disrupting public services, necessitating evacuations by civil protection teams, and resulting in significant material damages. Crucially, the flood-prone areas identified by LR and SVM models aligned remarkably well with the zones that experienced flooding during this event. The models mapped vulnerable areas offered an accuracy test in real-world conditions, underscoring their practical value in identifying and mitigating risks.

4. Discussion

Advanced statistical and machine learning models were used to assess urban flood vulnerability in the Tetouan-Martil region. Logistic Regression (LR) and Support Vector Machines (SVM) proved particularly effective, demonstrating high predictive accuracy. These results, validated through comparative analysis with other models such as Classification and Regression Trees (CART) and Factorial Discriminant Analysis (FDA), complement the findings of previous studies [12,46]. For instance, Sellami et al. [46] identified 32% of their study area as high-risk using SVM, an observation that closely aligns with our results, particularly in lowland areas with dense drainage networks. These outcomes confirm the robustness of our methodology and the reliability of AI/ML models for assessing urban flood vulnerability.

While the machine learning models used in this study demonstrated strong predictive performance, there are several limitations to consider. One primary challenge lies in the globality of the models. Our current approach was designed (e.g., type of chosen factors) specifically for the Tetouan-Martil region, and its applicability to other areas, particularly those with different topographies or urban planning, needs further validation. Testing these models on a broader scale, including various cities and watersheds in northern Morocco, will help assess their robustness and adaptability to different geographical and socio-economic contexts. Additionally, the model's reliance on the selected variables geo-environmental and socio-environmental could be expanded to incorporate more dynamic or real-time data sources. This could include data on rapid urbanization or instantaneous meteorological events, which would further refine the models' predictive power. We plan to explore these avenues in future work, seeking to integrate more comprehensive data sets to improve the accuracy and real-time applicability of the flood predictions.

The integration of Artificial Intelligence (AI) and Machine Learning (ML) into flood risk assessments represents a significant advancement in predictive accuracy and offers substantial benefits for real-time decision-making. Techniques such as Artificial Neural Networks (ANNs), Decision Trees (DTs), Convolutional Neural Networks (CNNs), and Random Forests (RFs) have proven effective in modelling complex flood patterns by leveraging diverse datasets, including historical flood records, remote sensing images, and socio-economic variables [47]. For example, CNNs and RFs have been successfully applied to accurately map flood risk zones in Beijing [48] and predict flood events. Although AI/ML models depend on the quality of training datasets, their ability to bridge gaps in flood mapping and provide real-time predictions is invaluable, particularly in dynamic urban environments such as Tetouan-Martil. These approaches compensate for incomplete drainage data by extracting meaningful patterns from heterogeneous datasets. The hybrid methodology, combining AI/ML techniques with traditional statistical models, ensures a robust analysis, while validation using the Repeated Hold-Out method further enhances the reliability of our findings.

Our study is based on 13 variables (nine geo-environmental and four socio-environmental), which may carry some redundant information. A preliminary step could have involved reducing data dimensionality through techniques such as Principal Component Analysis (PCA) or stepwise regression [49], thus preserving key socio-economic and infrastructural variables in the form of macro-parameters ("principal components") [50]. Although this particular approach in question was not adopted in this study, it could enhance flood risk maps by eliminating redundant data without compromising the analysis's relevance.

The combined impacts of climate change and urbanisation [51] on flood risks are evident in Mediterranean regions, including northern Morocco. Recent events in Spain, particularly in the provinces of Valencia and Catalonia in October 2024, serve as stark

reminders. Increasing short-duration, intense rainfall and unplanned urban expansion exacerbate flooding, particularly in low-lying areas with inadequate drainage infrastructure. Climatic factors such as heavy rainfall, rising temperatures, and sea-level rise, combined with rapid urban growth, significantly intensify urban flood risks [52]. Furthermore, regional topography, characterised by steep upstream areas and flat downstream plains prone to flash flooding, compounds these vulnerabilities [53].

These challenges are further exacerbated by socio-economic factors. High illiteracy rates, rapid demographic growth, and the settlement of populations in low-lying areas lacking adequate drainage infrastructure increase risks for marginalised communities [54]. These vulnerable communities, often situated in poorly equipped areas, suffer disproportionately during flood events [55].

Addressing these challenges requires an integrated and adaptive approach to urban flood management. This involves combining structural measures, such as improving drainage infrastructure and reducing impermeable surfaces, with non-structural interventions, such as sustainable land-use practices to preserve natural floodplains. However, these physical measures alone cannot fully mitigate flood risks without considering the socio-economic factors that exacerbate vulnerabilities. Prioritising the most vulnerable populations in flood management strategies, enhancing access to shelters, and strengthening community resilience are crucial. Climate projections must also inform flood models to anticipate future risks [52]. Finally, sustainable solutions, such as Blue-Green Infrastructure (BGI) and Sustainable Drainage Systems (SuDS), will play a key role in reducing flood risks and enhancing urban resilience.

Another important area for future development is incorporating long-term climate projections. While the current study focuses on historical data, integrating future climate scenarios will allow us to evaluate flood risks under changing environmental conditions, such as more intense rainfall and rising temperatures, which could significantly alter flood patterns. Future work will thus aim to develop adaptive models that not only predict current flood risks but also anticipate future challenges driven by climate change. Ultimately, the goal is to expand these models to regional and watershed scales, allowing for a more holistic and predictive approach to flood risk management across northern Morocco. This will be a key next step in ensuring the models' utility for large-scale urban planning and disaster prevention.

5. Conclusions

The urban flood vulnerability maps generated by the CART, SVM, LR, and FDA models exhibit a consistent pattern of flood vulnerability within the Tetouan-Martil study area. These maps indicate that flood-prone zones are predominantly located along the Martil River and in the eastern plains. Low-lying areas, high drainage density, proximity to canals, and the presence of newer buildings characterize these regions. Despite variations in spatial detail among the models, there is general agreement on the extent of low and very high flood vulnerability areas. Notably, the FDA model tends to overestimate the very high vulnerability zones, estimating that 58% of the area is at very high flood risk, in contrast to the LR, SVM, and CART models, which estimate approximately 37–39%. These findings offer valuable insights for urban planning and flood management strategies in the Tetouan-Martil area. The assessment of explanatory variables in susceptibility mapping enhances our understanding of urban flood vulnerability and supports resource allocation and management planning. While the susceptibility zones identified by the models are similar, the key contributing parameters differ. The FDA model emphasizes elevation, slope, and drainage density; the LR model highlights elevation, slope, exposition, and curvature; the CART model identifies elevation as the most influential factor; and the SVM

model points to drainage density, elevation, exposition, and slope. Interestingly, socio-environmental factors have minimal significance in susceptibility modelling for all four models. Understanding these contributing factors facilitates informed decision-making for resource allocation and flood risk management strategies. The study's results support the decision-making processes of authorities and policymakers in formulating policies aimed at reducing urban flood risk through sustainable urban management. These findings should be utilized for initial assessments of areas susceptible to fluvial flooding, guiding further analyses such as hydrodynamic modelling to understand flow conditions, including depth and velocity. However, reducing vulnerability to flood risk should not entail restricting high-risk areas but rather managing urbanization in these areas while encouraging development in already urbanized or less exposed regions. The research methodology employed in this study can be applied to other urban areas to aid in managing, controlling, and minimizing damage in flood-prone locations.

Author Contributions: Conceptualization, M.M. and T.B.; methodology, T.B. and O.M.; software, O.M.; validation, T.B., M.H. and H.A.; formal analysis, O.M. and R.P.M.R.; investigation, O.M.; resources, L.B. and M.M.; data curation, T.B. and M.H.; writing—original draft preparation, O.M., T.B. and M.M.; writing—review and editing, L.B. and O.M.; visualization, O.M. and T.B.; supervision, T.B. and M.M.; project administration, M.M. All authors have read and agreed to the published version of the manuscript.

Funding: This research received no external funding.

Data Availability Statement: Data are available in request.

Conflicts of Interest: The authors declare no conflicts of interest.

References

- Alexander, M.; Viavattene, C.; Faulkner, H.; Priest, S. *A GIS-Based Flood Risk Assessment Tool: Supporting Flood Incident Management at the Local Scale*; Flood Hazard Research Centre, Middlesex University: London, UK, 2011.
- Hossain, M.K.; Meng, Q. A Fine-Scale Spatial Analytics of the Assessment and Mapping of Buildings and Population at Different Risk Levels of Urban Flood. *Land Use Policy* **2020**, *99*, 104829. [\[CrossRef\]](#)
- Niculescu, S. Risque d'inondation dans le Delta du Danube. In *Festival International de Géographie, «La Planète en mal D'énergie»*; FIG: St Dié des Vosges, France, 2007.
- Svetlana, D.; Radovan, D.; Ján, D. The Economic Impact of Floods and Their Importance in Different Regions of the World with Emphasis on Europe. *Procedia Econ. Financ.* **2015**, *34*, 649–655. [\[CrossRef\]](#)
- Wood, H.M.; Lauritson, L. The CEOS Disaster Management Support Group. In Proceedings of the IGARSS 2000. IEEE 2000 International Geoscience and Remote Sensing Symposium. Taking the Pulse of the Planet: The Role of Remote Sensing in Managing the Environment. Proceedings (Cat. No. 00CH37120), Honolulu, HI, USA, 24–28 July 2000; IEEE: New York, NY, USA, 2000; Volume 6, pp. 2690–2692.
- United Nations. United Nations Office for Disaster Risk Reduction An Overview of the Last 20 Years. *Personal. Soc. Psychol. Bull.* **2020**, *21*, 324–343.
- Shaw, R.; Surjan, A.; Parvin, G.A. Urban disasters and approaches to resilience. In *Urban Disasters and Resilience in Asia*; Butterworth-Heinemann: Oxford, UK, 2016; pp. 1–19. ISBN 978-0-12-802169-9.
- Handayani, W.; Chigbu, U.E.; Rudiarto, I.; Putri, I.H. Urbanization and Increasing Flood Risk in the Northern Coast of Central Java—Indonesia: An Assessment towards Better Land Use Policy and Flood Management. *Land* **2020**, *9*, 343. [\[CrossRef\]](#)
- Manandhar, B.; Cui, S.; Wang, L.; Shrestha, S. Urban Flood Hazard Assessment and Management Practices in South Asia: A Review. *Land* **2023**, *12*, 627. [\[CrossRef\]](#)
- Miller, J.D.; Hutchins, M. The Impacts of Urbanisation and Climate Change on Urban Flooding and Urban Water Quality: A Review of the Evidence Concerning the United Kingdom. *J. Hydrol. Reg. Stud.* **2017**, *12*, 345–362. [\[CrossRef\]](#)
- Chauhan, S.; Dongol, R.; Chauhan, R. Evaluation of Economic Loss of Urban Road Flooding: A Case of Kathmandu Metropolitan City. *Environ. Chall.* **2023**, *13*, 100773. [\[CrossRef\]](#)
- Bouramtane, T.; Kacimi, I.; Bouramtane, K.; Aziz, M.; Abraham, S.; Omari, K.; Valles, V.; Leblanc, M.; Kassou, N.; El Beqqali, O.; et al. Multivariate Analysis and Machine Learning Approach for Mapping the Variability and Vulnerability of Urban Flooding: The Case of Tangier City, Morocco. *Hydrology* **2021**, *8*, 182. [\[CrossRef\]](#)

13. Pateau, M. De l'aléa Au Risque Naturel: Cas de La Région Tanger-Tétouan (Rif, Maroc). *Geo. Eco. Trop.* **2014**, *38*, 23–32.
14. Pateau, M. Le Complexe Portuaire «Tanger Med»: Une Stratégie Économique Aux Dépens d'une Gestion Durable Des Risques Naturels. *Bull. L'association Géographes Français Géographies* **2014**, *91*, 389–400. [\[CrossRef\]](#)
15. Agharroud, K.; Puddu, M.; Ivčević, A.; Satta, A.; Kolker, A.S.; Snoussi, M. Climate Risk Assessment of the Tangier-Tetouan-Al Hoceima Coastal Region (Morocco). *Front. Mar. Sci.* **2023**, *10*, 1176350. [\[CrossRef\]](#)
16. Ivčević, A.; Bertoldo, R.; Mazurek, H.; Siame, L.; Guignard, S.; Moussa, A.B.; Bellier, O. Local Risk Awareness and Precautionary Behaviour in a Multi-Hazard Region of North Morocco. *Int. J. Disaster Risk Reduct.* **2020**, *50*, 101724. [\[CrossRef\]](#)
17. Ayalew, L.; Yamagishi, H. The Application of GIS-Based Logistic Regression for Landslide Susceptibility Mapping in the Kakuda-Yahiko Mountains, Central Japan. *Geomorphology* **2005**, *65*, 15–31. [\[CrossRef\]](#)
18. AL-Hussein, A.A.M.; Khan, S.; Ncibi, K.; Hamdi, N.; Hamed, Y. Flood Analysis Using HEC-RAS and HEC-HMS: A Case Study of Khazir River (Middle East—Northern Iraq). *Water* **2022**, *14*, 3779. [\[CrossRef\]](#)
19. Syarifudin, A.; Satyanaga, A.; Destania, H.R. Application of the HEC-RAS Program in the Simulation of the Streamflow Hydrograph for Air Lakitan Watershed. *Water* **2022**, *14*, 4094. [\[CrossRef\]](#)
20. Azouagh, A.; Bardai, R.; Hilal, I.; Messari, J. Integration of GIS and HEC-RAS in Floods Modeling of Martil River (Northern Morocco). *Eur. Sci. J.* **2018**, *14*, 130–142. [\[CrossRef\]](#)
21. Karrouchi, M.; Touhami, M.O.; Oujidi, M.; Chourak, M. Mapping of Flooding Risk Areas in the Tangier-Tetouan Region: Case of Martil Watershed (Northern Morocco). *Int. J. Innov. Appl. Stud.* **2016**, *14*, 1019–1035.
22. Mosavi, A.; Ozturk, P.; Chau, K. Flood Prediction Using Machine Learning Models: Literature Review. *Water* **2018**, *10*, 1536. [\[CrossRef\]](#)
23. Motta, M.; de Castro Neto, M.; Sarmiento, P. A Mixed Approach for Urban Flood Prediction Using Machine Learning and GIS. *Int. J. Disaster Risk Reduct.* **2021**, *56*, 102154. [\[CrossRef\]](#)
24. Choubin, B.; Moradi, E.; Golshan, M.; Adamowski, J.; Sajedi-Hosseini, F.; Mosavi, A. An Ensemble Prediction of Flood Susceptibility Using Multivariate Discriminant Analysis, Classification and Regression Trees, and Support Vector Machines. *Sci. Total Environ.* **2019**, *651*, 2087–2096. [\[CrossRef\]](#)
25. HCP. Monographie de la Region Tanger-Tetouan-Al Hoceima. *Haut Commis. Au Plan* **2020**, 236.
26. Prokos, H.; Baba, H.; LóCzy, D.; El Kharim, Y. Geomorphological Hazards in a Mediterranean Mountain Environment-Example of Tétouan, Morocco. *Hung. Geogr. Bull.* **2016**, *65*, 283–295. [\[CrossRef\]](#)
27. Morabiti, K.; El Kharim, Y. Etude Hydrogéologique et Hydrogéochimique Des Principales Sources Karstiques Dans Les Environs de La Ville de Tétouan. *Rev. AFN Maroc* **2009**, *4–5*, 58–69.
28. Azzouz, O.; El Fellah, B.; Chalouan, A. Processus de Glissement Dans Le Massif de Bokoya (Rif Interne, Maroc): Exemple de Cala Bonita. *Bull. L'institut Sci. Rabat Sect. Sci. La Terre* **2002**, *24*, 33–40.
29. Benzécri, J.-P. Analyse Discriminante et Analyse Factorielle. *Cah. L'analyse Des Données* **1977**, *2*, 369–406.
30. Chavent, M. Analyse Factorielle Discriminante (AFD). *Dim* **2016**, *1*, 18–49.
31. Breiman, L. *Classification and Regression Trees*; Routledge: London, UK, 2017; ISBN 1315139472.
32. Breiman, L.; Friedman, J.; Olshen, R.; Stone, C. *Classification and Regression Trees*; Wadsworth: Monterey, CA, USA, 1984.
33. Pham, B.T.; Prakash, I.; Bui, D.T. Spatial Prediction of Landslides Using a Hybrid Machine Learning Approach Based on Random Subspace and Classification and Regression Trees. *Geomorphology* **2018**, *303*, 256–270. [\[CrossRef\]](#)
34. Loh, W. Classification and Regression Trees. *Wiley Interdiscip. Rev. Data Min. Knowl. Discov.* **2011**, *1*, 14–23. [\[CrossRef\]](#)
35. Vapnik, V.N.; Chervonenkis, A.Y. On a Perceptron Class. *Autom. Remote Control* **1964**, *25*, 112–120.
36. Darabi, H.; Choubin, B.; Rahmati, O.; Haghighi, A.T.; Pradhan, B.; Kløve, B. Urban Flood Risk Mapping Using the GARP and QUEST Models: A Comparative Study of Machine Learning Techniques. *J. Hydrol.* **2019**, *569*, 142–154. [\[CrossRef\]](#)
37. Chen, W.; Peng, J.; Hong, H.; Shahabi, H.; Pradhan, B.; Liu, J.; Zhu, A.-X.; Pei, X.; Duan, Z. Landslide Susceptibility Modelling Using GIS-Based Machine Learning Techniques for Chongren County, Jiangxi Province, China. *Sci. Total Environ.* **2018**, *626*, 1121–1135. [\[CrossRef\]](#) [\[PubMed\]](#)
38. Tien Bui, D.; Pradhan, B.; Lofman, O.; Revhaug, I. Landslide Susceptibility Assessment in Vietnam Using Support Vector Machines, Decision Tree, and Naive Bayes Models. *Math. Probl. Eng.* **2012**, *2012*, 974638. [\[CrossRef\]](#)
39. Shmueli, G. To Explain or to Predict? *Stat. Sci.* **2010**, *25*, 289–310. [\[CrossRef\]](#)
40. Tanner, E.M.; Bornehag, C.-G.; Gennings, C. Repeated Holdout Validation for Weighted Quantile Sum Regression. *MethodsX* **2019**, *6*, 2855–2860. [\[CrossRef\]](#)
41. Monteiro, J.M.; Rao, A.; Shawe-Taylor, J.; Mourao-Miranda, J.; Initiative, A.D. A Multiple Hold-out Framework for Sparse Partial Least Squares. *J. Neurosci. Methods* **2016**, *271*, 182–194. [\[CrossRef\]](#)
42. Pal, K.; Patel, B.V. Data Classification with K-Fold Cross Validation and Holdout Accuracy Estimation Methods with 5 Different Machine Learning Techniques. In Proceedings of the 2020 Fourth International Conference on Computing Methodologies and Communication (ICCMC), Erode, India, 11–13 March 2020; IEEE: New York, NY, USA, 2020; pp. 83–87.

43. Bouramtane, T.; Hilal, H.; Rezende-Filho, A.T.; Bouramtane, K.; Barbiero, L.; Abraham, S.; Valles, V.; Kacimi, I.; Sanhaji, H.; Torres-Rondon, L. Mapping Gully Erosion Variability and Susceptibility Using Remote Sensing, Multivariate Statistical Analysis, and Machine Learning in South Mato Grosso, Brazil. *Geosciences* **2022**, *12*, 235. [\[CrossRef\]](#)
44. Marzban, C. The ROC Curve and the Area under It as Performance Measures. *Weather Forecast.* **2004**, *19*, 1106–1114. [\[CrossRef\]](#)
45. Efron, B. *The Jackknife, the Bootstrap and Other Resampling Plans*; SIAM: Philadelphia, PA, USA, 1982; ISBN 0898711797.
46. Sellami, E.M.; Maanan, M.; Rhinane, H. Performance of Machine Learning Algorithms for Mapping and Forecasting of Flash Flood Susceptibility in Tetouan, Morocco. *Int. Arch. Photogramm. Remote Sens. Spat. Inf. Sci.* **2022**, *46*, 305–313. [\[CrossRef\]](#)
47. Agonafir, C.; Lakhankar, T.; Khanbilvardi, R.; Krakauer, N.; Radell, D.; Devineni, N. A Review of Recent Advances in Urban Flood Research. *Water Secur.* **2023**, *19*, 100141. [\[CrossRef\]](#)
48. Zhao, G.; Pang, B.; Xu, Z.; Peng, D.; Zuo, D. Urban Flood Susceptibility Assessment Based on Convolutional Neural Networks. *J. Hydrol.* **2020**, *590*, 125235. [\[CrossRef\]](#)
49. Roldán-Valcarce, A.; Jato-Espino, D.; Manchado, C.; Bach, P.M.; Kuller, M. Vulnerability to Urban Flooding Assessed Based on Spatial Demographic, Socio-Economic and Infrastructure Inequalities. *Int. J. Disaster Risk Reduct.* **2023**, *95*, 103894. [\[CrossRef\]](#)
50. Tiouiouine, A.; Yameogo, S.; Valles, V.; Barbiero, L.; Dassonville, F.; Moulin, M.; Bouramtane, T.; Bahaj, T.; Morarech, M.; Kacimi, I. Dimension Reduction and Analysis of a 10-Year Physicochemical and Biological Water Database Applied to Water Resources Intended for Human Consumption in the Provence-Alpes-Cote d’Azur Region, France. *Water* **2020**, *12*, 525. [\[CrossRef\]](#)
51. Bagheri, A.; Liu, G.-J. Climate Change and Urban Flooding: Assessing Remote Sensing Data and Flood Modeling Techniques: A Comprehensive Review. *Environ. Rev.* **2025**, *33*, 1–14. [\[CrossRef\]](#)
52. O'Donnell, E.C.; Thorne, C.R. Drivers of Future Urban Flood Risk. *Philos. Trans. R. Soc. A* **2020**, *378*, 20190216. [\[CrossRef\]](#)
53. Feng, B.; Zhang, Y.; Bourke, R. Urbanization Impacts on Flood Risks Based on Urban Growth Data and Coupled Flood Models. *Nat. Hazards* **2021**, *106*, 613–627. [\[CrossRef\]](#)
54. Vousdoukas, M.I.; Mentaschi, L.; Voukouvalas, E.; Bianchi, A.; Dottori, F.; Feyen, L. Climatic and Socioeconomic Controls of Future Coastal Flood Risk in Europe. *Nat. Clim. Change* **2018**, *8*, 776–780. [\[CrossRef\]](#)
55. Ermagun, A.; Smith, V.; Janatabadi, F. High Urban Flood Risk and No Shelter Access Disproportionally Impacts Vulnerable Communities in the USA. *Commun. Earth Environ.* **2024**, *5*, 2. [\[CrossRef\]](#)

Disclaimer/Publisher’s Note: The statements, opinions and data contained in all publications are solely those of the individual author(s) and contributor(s) and not of MDPI and/or the editor(s). MDPI and/or the editor(s) disclaim responsibility for any injury to people or property resulting from any ideas, methods, instructions or products referred to in the content.